NUCLEAR TECHNOLOGY · VOLUME 193 · 161–174 · JANUARY 2016

BWR Station Blackout: A RISMC Analysis Using RAVEN and RELAP5-3D

D. Mandelli,* C. Smith, T. Riley, J. Nielsen, A. Alfonsi, J. Cogliati, C. Rabiti, and J. Schroeder

Idaho National Laboratory, 2525 North Fremont Avenue, Idaho Falls, Idaho 83415

Received December 12, 2014
Accepted for Publication May 8, 2015
http://dx.doi.org/10.13182/NT14-142

Abstract — *The existing fleet of nuclear power plants is in the process of having its lifetime extended and having the power generated from these plants increased via power uprates and improved operations. In order to evaluate the impact of these factors on the safety of the plant, the Risk-Informed Safety Margin Characterization (RISMC) pathway aims to provide insights to decision makers through a series of simulations of the plant dynamics for different initial conditions and accident scenarios. This paper presents a case study in order to show the capabilities of the RISMC methodology to assess the impact of power uprate of a boiling water reactor system during a station blackout accident scenario. We employ a system simulator code, RELAP5-3D, coupled with RAVEN, which performs the stochastic analysis. Our analysis is performed by (a) sampling values from a set of parameters from the uncertainty space of interest, (b) simulating the system behavior for that specific set of parameter values, and (c) analyzing the outcomes from the set of simulation runs.*

Keywords — *Dynamic PRA, safety margin, station blackout.*

Note — *Some figures may be in color only in the electronic version.*

I. INTRODUCTION

The Risk-Informed Safety Margin Characterization[1] (RISMC) pathway, as part of the Light Water Reactor Sustainability (LWRS) program,[2] aims to develop simulation-based tools and methods to assess risks for existing nuclear power plants (NPPs) in order to optimize safety. By developing new methods, this pathway is extending the probabilistic risk assessment (PRA) state-of-the-practice methods[3] that have been traditionally based on logic structures such as event trees (ETs) and fault trees (FTs) (Ref. 4). These static types of models mimic system response in an inductive way and a deductive way, respectively, yet are restrictive in the ways they can represent spatial and temporal constructs. Fault trees are used to build logical event relationships between basic events (typically representing component failures) that affect branching conditions in the ET.

*E-mail: diego.mandelli@inl.gov

The ET structure follows a precise logic that is defined a priori by the user; i.e., the sequences of events in the ET are fixed and not interchangeable (in other words, they are part of a static model represented by a simple Boolean logic expression). As indicated in the historical accident in the nuclear industry, the timing of occurrence of such events can play a major role in the accident evolution. This timing information is not implicitly considered in an ET-FT structure; it is in fact only loosely considered in the definition of the basic events, e.g., diesel generator (DG) recovery within 4 h.

Both these issues (fixed logic structure and lack of timing considerations) preclude the ability to fully analyze possible accident evolution trajectories and, thus, also the possibility to evaluate the importance of basic events in the overall core damage (CD) probability.

This is one reason why the RISMC pathway is employing state-of-the-art simulation-based methodologies coupled with probabilistic analysis tools to evaluate accident evolution and the risk associated with these sce-

narios. These issues are particularly relevant for RISMC, where it is needed to evaluate the impact of plant changes such as power uprates and life extension on existing NPPs. From an ET-FT logic point of view, both power uprate and life extensions are not modeled, which further shows the limitations of these kinds of methodologies for design and operational considerations.

Such deterministic-probabilistic coupling has been investigated and explored by several research groups such as the Organisation for Economic Co-operation and Development/Nuclear Energy Agency (NEA) Committee on the Safety of Nuclear Installations (CSNI) (Ref. 5), where the analysis framework proposed by the NEA-CSNI Action Plan on Safety Margins merges traditional deterministic and probabilistic (PRA) techniques. The Paul Scherrer Institute[6] has followed a similar path by employing dynamic ETs to evaluate operator actions during accident scenarios. Similarly, Électricité de France and The Ohio State University have recently developed such integration as discussed in Refs. 7 and 8, respectively. Last, a recent overview of integrated deterministic and probabilistic safety analysis can be found in Ref. 9.

The scopes of this paper are as follows:

1. Describe the RISMC approach in detail and, in particular, the software components that are employed and the steps required to perform RISMC analyses.

2. Show the RISMC approach applied to a boiling water reactor (BWR) station blackout (SBO) test case. Step by step, it will be shown how the components required by the RISMC approach are employed.

II. RISMC SIMULATION-BASED APPROACH

The RISMC pathway uses the probabilistic margin approach to quantify impacts to reliability and safety. As part of the quantification, we use both probabilistic (via risk simulation) and mechanistic (via physics models) approaches, as represented in Fig. 1. Probabilistic analysis is represented by the risk analysis while mechanistic analysis is represented by the plant physics calculations. Safety margin and uncertainty quantification rely on plant physics [e.g., thermal-hydraulic codes such as RELAP5-3D (Ref. 10) and RELAP-7 (Ref. 11) or component-aging modeling codes such as GRIZZLY (Ref. 12)] coupled with probabilistic risk simulation–stochastic analysis tools [i.e., RAVEN (Ref. 13)]. The coupling takes place through the interchange of physical parameters (e.g., pressures and temperatures) and operational or accident scenarios.

In Sec. I, we have shown the main reasons behind the choice of moving from an ET-FT logic structure and directly employing system simulator codes to perform PRA analyses. A single simulation can be seen as single trajectory in the system phase-space. The evolution of such trajectory in phase-space can be described as follows:

$$\frac{\partial \theta(t)}{\partial t} = \mathcal{H}(\theta, \boldsymbol{s}, t) , \tag{1}$$

where

$\theta = \theta(t)$ = status of the system as a function of time t; i.e., $\theta(t)$ represents a single simulation

$\mathcal{H}$ = actual simulator code that describes how θ evolves in time

$s = s(t)$ = status of components and systems of the simulator [e.g., status of emergency core cooling system (ECCS), alternating-current (AC) system].

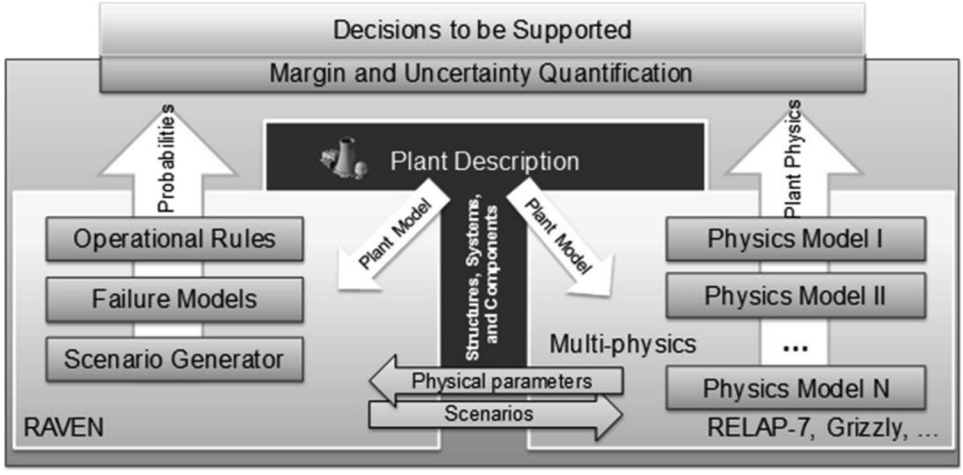

Fig. 1. Overview of the RISMC approach.

By using the RISMC approach, the PRA analysis is performed by

1. associating a probabilistic distribution function (pdf) to the set of parameters s (e.g., timing of events)
2. performing sampling of the pdf's defined in step 1
3. performing a simulation run given s sampled in step 2; i.e., solve Eq. (1)
4. repeating steps 2 and 3 N times and evaluating user-defined stochastic parameters such as CD probability (P_{CD}).

In order to perform PRA analyses of NPPs, the RISMC pathway employs the RAVEN statistical framework,[13] which is a recent add-on of the RAVEN package,[14] that allows the user to perform generic statistical analysis. By statistical analysis we include sampling of codes [e.g., Monte Carlo[15] and Latin hypercube sampling,[16] grid sampling, and dynamic ET (Ref. 17)], generation of reduced-order models[18] (ROMs) (also known as surrogate models or emulators), postprocessing of the sampled data, and generation of statistical parameters (e.g., mean, variance, and covariance matrix).

Figure 2 shows an overview of the elements that comprise the RAVEN statistical framework:

1. *Model:* It represents the pipeline between the input and output spaces. It comprises both interfaces for mechanistic codes [e.g., RELAP5-3D (Ref. 10) and RELAP-7 (Ref. 11)] and ROMs.

2. *Sampler:* It is the driver for any specific sampling strategy [e.g., Monte Carlo,[19] Latin hypercube sampling,[20] dynamic ET (Ref. 21)].

3. *Database:* It is the data storing entity.

4. *Postprocessing:* It is the module that performs statistical analyses and visualizes results.

RAVEN is interfaced with several codes, and actually, the user can build its own interface for the code that he or she is interested in running. The interface for RELAP5-3D allows RAVEN to change specific values of any card contained in the RELAP5-3D input files accordingly to the chosen sampling strategy.

In addition, at the end of each RELAP5-3D simulation run, RAVEN collects and stores all information generated from the output files (in the database manager), generates CSV (comma separated values) files of the output data, and processes such data through its internal postprocessing and data mining module.

If multiple simulations need to be run, RAVEN has the capability to run simulations in parallel on multiple nodes and/or multiple CPUs. RAVEN applicability ranges from Linux-based desktop/laptop to high-performance computing machines.

As mentioned earlier, RAVEN also has the capability to "train" ROMs from any data set generated by any codes. These ROMs are usually a blend of interpolation and regression algorithms, and such a "training process" basically consists of setting the optimal parameters of the interpolation and regression algorithms that best fit the

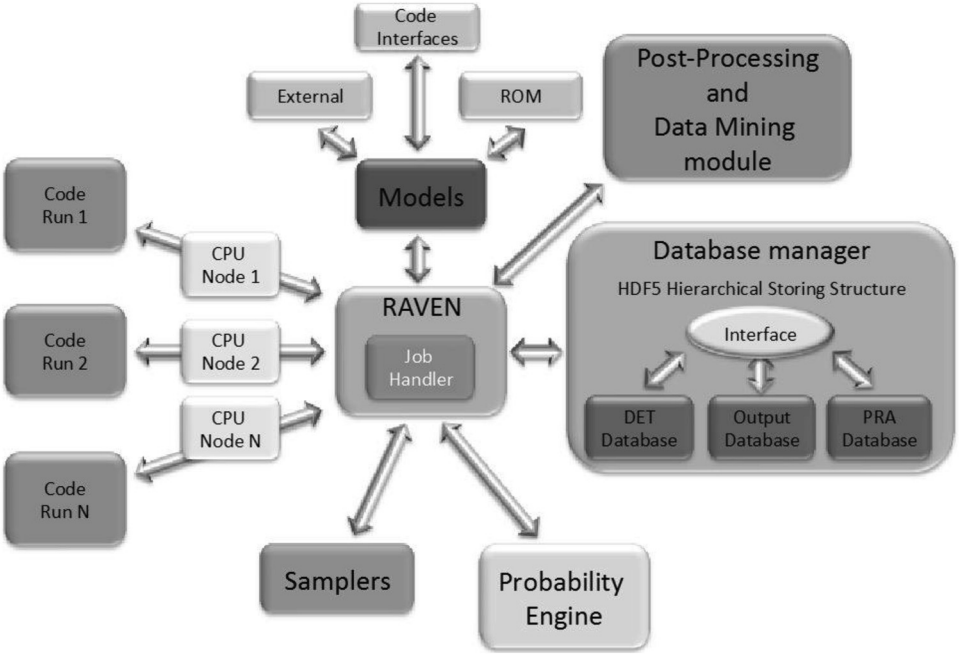

Fig. 2. Structure of RAVEN statistical framework components.

input data set. Once the ROMs are generated, they can be used instead of the actual codes to perform any type of analysis since the generation of data from ROM is much faster than the original code.

In a typical RISMC-type analysis, the user specifies in the RAVEN input file not only where the RELAP5-3D executable files and the input files are located, but also the probabilistic distribution for each uncertain parameter and where such parameter needs to be changed in the RELAP5-3D input file. Afterward, the user specifies which sampling strategy has been chosen, what output variables need to be retrieved (and subsequently stored in the RAVEN database) from the RELAP5-3D output files, and which postprocessing functions of the output data are required.

III. BWR SBO TEST CASE

III.A. BWR Model

The system considered in this test case is a generic BWR NPP with a Mark I containment as shown in Fig. 3a. The main structures are the following[22]: reactor pressure vessel (RPV), the pressurized vessel that contains the reactor core, and the primary containment. The primary containment includes the drywell (DW); the pressure suppression pool (PSP), also known as wetwell; and the reactor circulation pumps. The PSP is a large torus-shaped container that contains a large amount of water that is used as ultimate heat sink.

Three sources of core cooling water inventory are available:

1. condensate storage tank (CST), which contains freshwater that can be used to cool the reactor core
2. PSP, which contains a large amount of freshwater that is used to provide temporary and finite heat sink when AC power is lost
3. firewater (FW) system: water contained in the FW system can be injected into the RPV when other water injection systems are disabled and when RPV is depressurized.

The high-pressure RPV level control is provided by two systems: the reactor core isolation cooling (RCIC) system and the high pressure coolant injection (HPCI) system. RCIC provides high-pressure injection of water from the CST to the RPV. Water flow from the CST to the RPV is provided by a turbine-driven pump that takes steam from the main steam line and discharges it to the PSP. Alternatively, the water source can be shifted from the CST to the PSP. HPCI is similar to RCIC, but it allows greater water flow rates. Note that RCIC and HPCI cannot both be employed if the RPV is depressurized.

The RPV pressure control is provided by the safety relief valves (SRVs) and the automatic depressurization system (ADS). SRVs are direct-current (DC)–powered valves that control and limit the RPV pressure within 900 and 1100 psi. The ADS consists of a separate set of

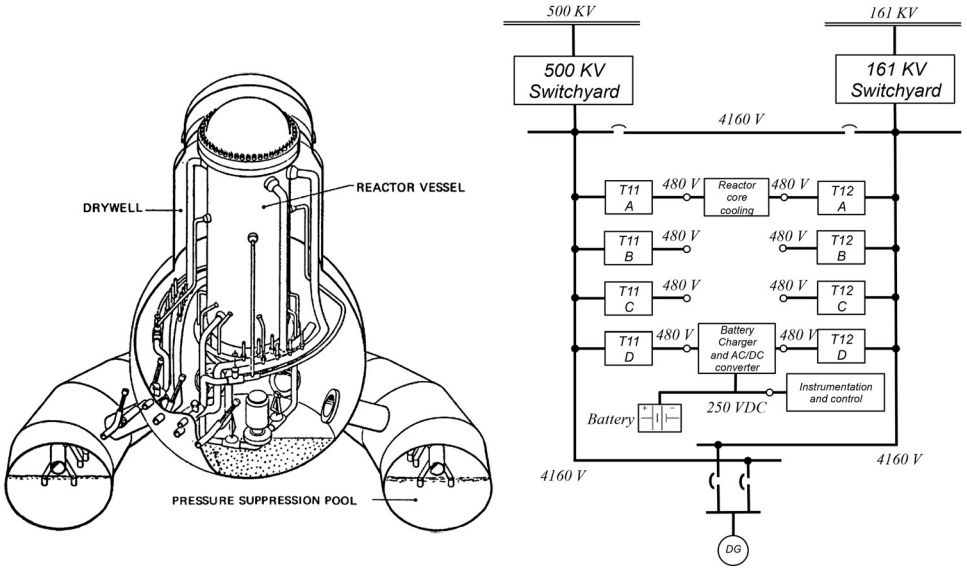

(a) (b)

Fig. 3. Overview of the BWR system with (a) Mark I (Ref. 23) and (b) AC/DC power system schematics.

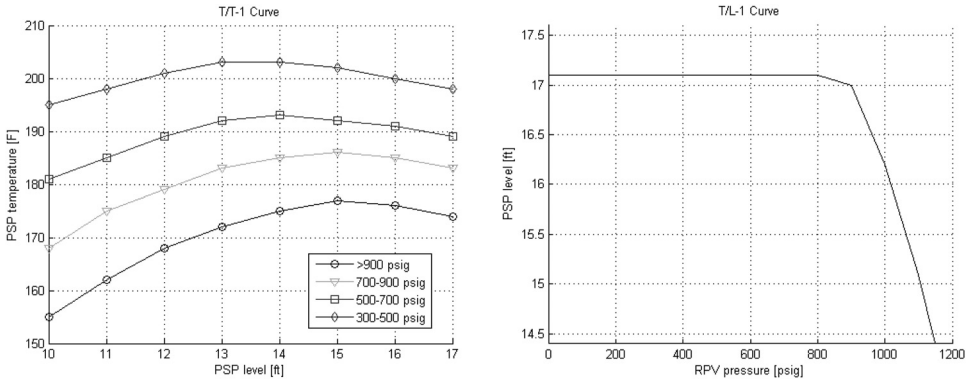

Fig. 4. HCTL curves for PSP.

relief valves that are employed to completely depressurize the RPV.

Several power systems are also included in the BWR model (see Fig. 3b):

1. two independent power grids (PGs) that are connected to the plant station through two independent switchyards (500 KV and 161 KV)
2. diesel generators that provide emergency AC power if PG power is not available
3. battery systems that provide DC power to instrumentation and control systems.

Complete loss of AC power disables the operability of all systems except ADS, SRV, RCIC, and HPCI (which requires only a DC battery).

In an accident scenario, the set of emergency operating procedures requires the reactor operators to monitor not only the RPV but also the containment (both DW and PSP) thermohydraulic parameters (level, pressure, and temperature). In this respect, a set of limit curves is provided to the reactor operator so that when they are crossed, the operators are required to activate the ADS. These limit curves, also known as heat capacity temperature limits (HCTLs), are shown in Figs. 4 and 5 for both PSP and DW, respectively.

After ADS activation, no reactor core cooling is available unless AC power is recovered; alternatively, FW can be aligned to the RPV in order to provide core cooling.

The BWR dynamic has been modeled using RELAP-5. The system nodalization is shown in Fig. 6 and includes

1. RPV components such as the reactor core, downcomer, steam dome, jet pump, SRVs, and ADS
2. containment components such as PSP, DW, recirculation pumps, and CST
3. external systems such as RCIC, HPCI, and FW.

For the scope of this analysis, we have decided to stop the simulation when one these three stopping conditions is met:

1. Clad temperature reaches clad failure temperature.
2. Alternating-current power is recovered.
3. Firewater is available.

The fact that one of the stopping conditions is "clad temperature reaches clad failure temperature" implies that our analysis does not cover any type of severe accident phenomenon; i.e., the analysis presented in this paper can be considered a Level 1 PRA analysis.

III.B. SBO Scenario

The accident scenario under consideration is a loss of off-site power (LOOP) followed by loss of the DGs, i.e.,

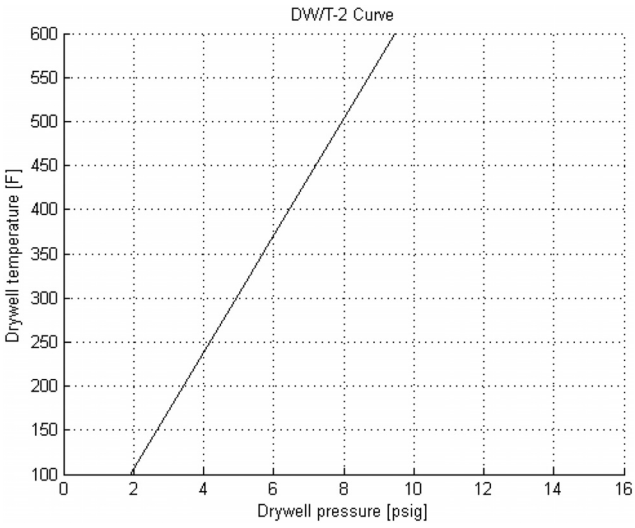

Fig. 5. HCTL curve for DW.

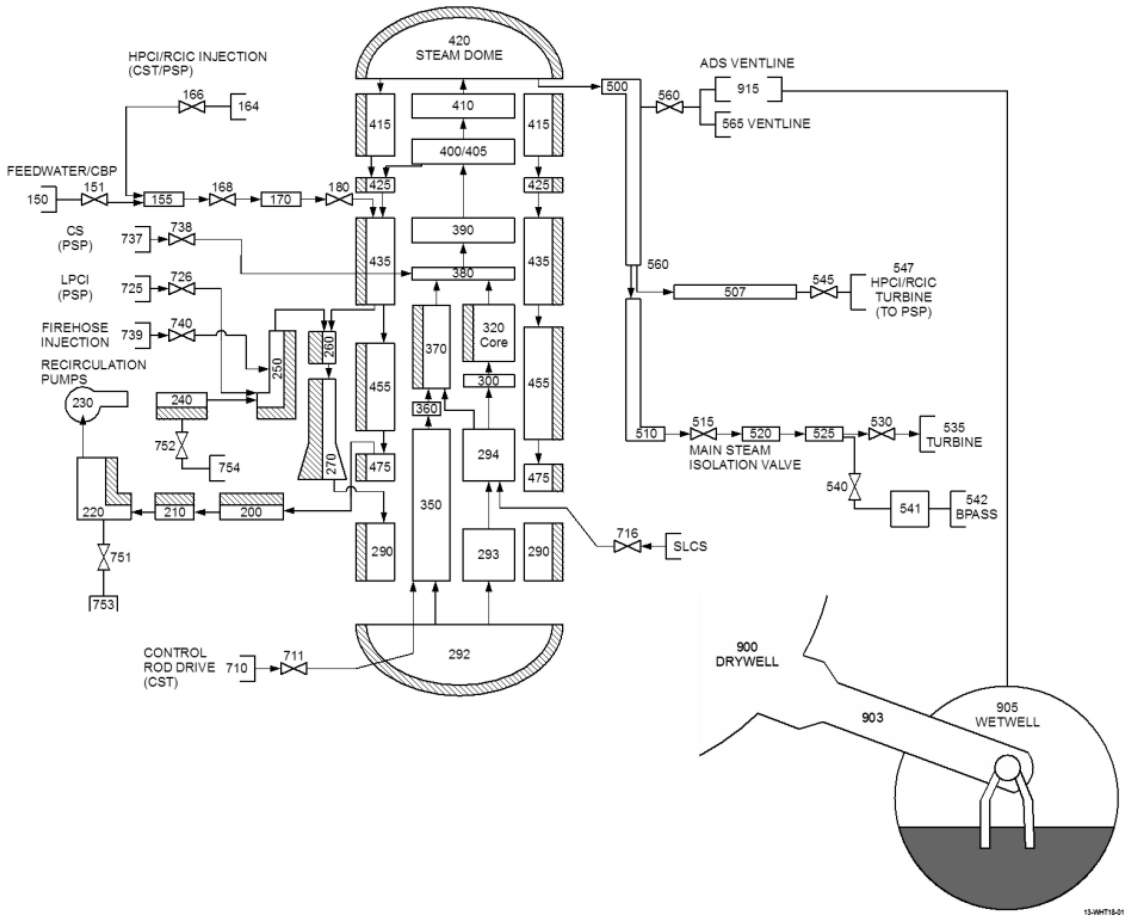

Fig. 6. RELAP5-3D nodalization of the BWR system.

SBO initiating event. In more detail, at time $t = 0$ the LOOP condition occurs due to external events (i.e., PG related), which triggers the following actions:

1. Operators successfully scram the reactor and put it in subcritical conditions by fully inserting the control rods into the core.

2. Emergency DGs successfully start; i.e., AC power is available.

3. Core decay heat is removed from the RPV through the residual heat removal system.

4. Direct-current systems (i.e., batteries) are functional.

At an uncertain time, the SBO condition occurs: Because of internal failure, the set of DGs fails. Thus, removal of decay heat is impeded. Reactor operators start the SBO emergency operating procedures and perform the following:

1. RPV level control using RCIC or HPCI

2. RPV pressure control using SRVs

3. containment monitoring (both DW and PSP).

At the same time, plant operators start recovery operations to bring back online the DGs while the recovery of the PG is underway by the grid owner emergency staff.

Because of the limited life of the battery system and depending on the use of DC power, battery power can deplete. When this happens, all remaining control systems are off-line, causing the reactor core to heat until the clad failure temperature is reached, i.e., CD.

If DC power is still available and one of the following conditions is reached:

1. failure of both RCIC and HPCI

2. HCTLs reached

3. low RPV water level,

then the reactor operators activate the ADS system in order to depressurize the RPV.

As an emergency action, when the RPV pressure is below 100 psi, plant staff can connect the FW system to the RPV in order to cool the core and maintain an adequate water level. Such task is, however, hard to complete since physical connection between the FW system and the RPV inlet has to be made manually. For our case study,

since our simulations stop when a specific stopping condition is met (plant AC power is recovered or FW is available or maximum clad temperature reaches clad fail temperature), FW recovery can happen only before CD (i.e., severe accident phenomena are not considered).

When AC power is recovered, through successful restart/repair of DGs or off-site PG, auxiliary core cooling can now be employed to keep the reactor core cool.

As an example of the BWR SBO scenario, we performed a single simulation run in which the SBO condition occurred 3 h after LOOP and a failure in the DC system occurred 4700 s following the SBO event (such a scenario is shown in Fig. 7):

1. Following a failure to run the DGs, the RPV pressure increases while the RPV water level decreases. This triggers activation of both RCIC and SRVs.

2. Cycling of SRVs causes the PSP temperature to increase at each SRV activation. In our analysis it is assumed that there is no spatial gradient in the initial PSP temperature.

3. RCIC activation causes the RPV pressure to drop and the RPV level to increase.

4. Loss of the DC battery makes it impossible to control both the RPV level and pressure. While the RPV level decreases, the pressure is kept steady at ~1105 psi due to continued cycling of the RPV safety valves (automatic activation for RPV pressure >1105 psi).

III.C. Stochastic Parameters

For this analysis we considered several uncertain parameters; the choice of such parameters has been based on classical PRA studies that analyzed similar accident scenarios such as NUREG-1150 (Ref. 3). Obviously, such a set of parameters is not exhaustive and could be easily expanded if more phenomena need to be modeled. These parameters are as follows:

1. *Failure time of DGs*: Regarding the time at which the DGs fail to run, we chose an exponential distribution with a value of lambda equal to 1.09×10^{-3} h^{-1}.

2. *Recovery time of DGs*: Regarding the time needed to recover the DGs, we used as a reference NUREG/CR-6890, Vol. 1 (Ref. 24). This document uses a Weibull distribution[a] with $\alpha = 0.745$ and $\beta = 6.14$ h (mean = 7.4 h and median = 3.8 h). Such a distribution represents the

[a]Weibull distribution pdf(x) is here defined as pdf(x) = $(\alpha/\beta^{\alpha})x^{\alpha-1}e^{-(x/\beta)^{\alpha}}$.

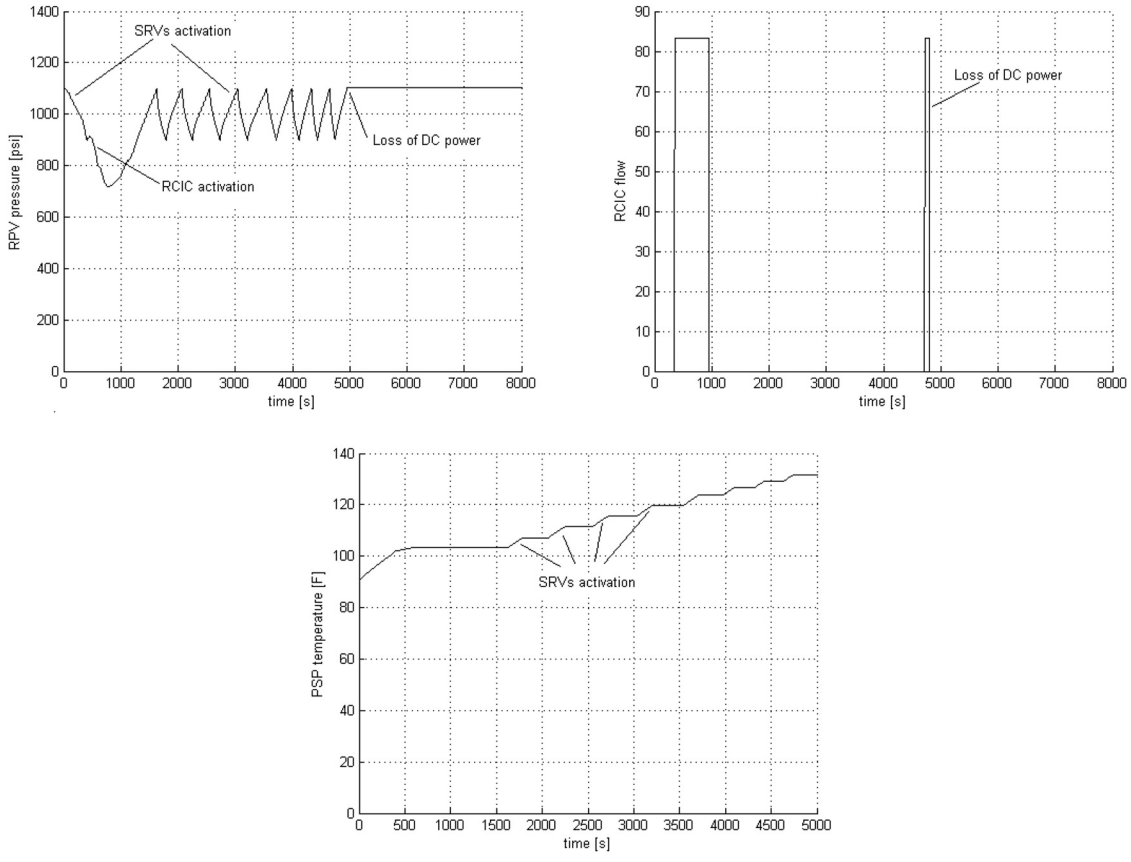

Fig. 7. Example of BWR SBO scenario.

pdf of repair of one of the two DGs (choosing the one easiest to repair).

3. *Off-site AC power recovery*: For the time needed to recover the off-site PG, we used as reference NUREG/CR-6890, Vol. 2 (Ref. 25) (data collection was performed between 1986 and 2004). Given the four possible LOOP categories (plant centered, switchyard centered, grid related, or weather related), severe/extreme events (such as earthquake) are assumed to be similar to these events found in the weather category (these are typically long-term types of recoveries). This category is represented with a lognormal distribution [from NUREG/CR-6890 (Ref. 25)] with $\mu = 0.793$ and $\sigma = 1.982$.

4. *Battery life*: For the amount of DC power available, when AC power is not obtainable, we chose to limit the battery life between 4 and 6 h using a triangular distribution [see NUREG/CR-6890, Vol. 2 (Ref. 25)].

5. *Battery failure time*: As a basic event in the PRA model, the probability value associated with battery failure is equal to 1.4×10^{-5} for an expected life of 4 h. We have assumed an exponential distribution for the battery failure time distribution. The value of λ for this distribution has been calculated by imposing the cumulative distribution function of this distribution ($1 - e^{-\lambda t}$) at 4 h (i.e., the probability that the battery fails within 4 h is 1.4×10^{-5}):

$$\int_0^4 \lambda e^{-\lambda t} dt = [1 - e^{-\lambda t}]_0^4 = 1.4 \times 10^{-5} .$$

This leads to a value of $\lambda = 3.5 \times 10^{-6}$/h.

6. *SRVs fail open*: The model used for this event has a probability value on demand of 8.56×10^{-4}.

7. *Clad fail temperature*: Uncertainty in failure temperature for the clad is characterized by a triangular distribution[26] having

a. lower limit = 1800°F (982°C): PRA success criterion

b. upper limit = 2600°F (1427°C): Urbanic-Heidrick transition temperature

c. mode = 2200°F (1204°C): 10 CFR regulatory limit.

8. *RCIC fails to run*: Regarding the distribution of RCIC to fail to run, we assumed an exponential distribution with a rate of 4.43×10^{-3}/h.

9. *HPCI fails to run*: Regarding the distribution of HPCI to fail to run, we assumed an exponential distribution with a rate of 4.43×10^{-3}/h.

10. *Firewater flow rate*: The value of the FW flow rate is between 150 and 300 gal/min (Ref. 27). For the scope of this paper, we also considered the possibility of very low FW flow rates. Thus, we assumed a triangular distribution defined in the interval [0,300] gal/min with mode at 200 gal/min.

Regarding the pdf's related to human-related actions, we looked into the SPAR-H model.[28] SPAR-H characterizes each operator action through eight parameters. For this study we focused on the two important factors: stress/stressor level and task complexity.

These two parameters are used to compute the probability that such action will happen or not; these probability values are then inserted into the ETs that contain these events. However, from a simulation point of view, we are not seeking if an action is performed but rather when such action is performed. Thus, we need a pdf that defines the probability that such action will occur as a function of time.

Since modeling of human actions is often performed using lognormal distributions,[25] we chose such a distribution where its character parameters (i.e., μ and σ) are dependent on the two factors listed above (stress/stressor level and task complexity). We used Table I (Ref. 29) to convert the three possible values of the two factors into numerical values for μ and σ.

For our specific case we modeled two human-related actions indicated as follows:

1. *Battery repair time*: Direct-current battery system restoration is performed by recovering batteries from nearby vehicles and connecting them to the plant DC system. We assumed that this task has high complexity with an extreme stress/stressor level. This leads to $\mu = 45$ min and $\sigma = 15$ min.

2. *Firewater availability time*: The operations to align the FW system to the RPV are considered very complex. This time is measured after the ADS has been activated, i.e., after the RPV has been depressurized. Also, for this case we assumed that this task has a high complexity with an extreme stress/stressor level. This leads to $\mu = 45$ min and $\sigma = 30$ min.

TABLE I

Correspondence Table Between Complexity and Stress/Stressor Level and Time Values

Complexity	μ (min)	Stress/Stressor Level	σ (min)
High	45	Extreme	30
Moderate	15	High	15
Nominal	5	Nominal	5

TABLE II

Summary of the Stochastic Parameters and Their Associated Distributions

Stochastic Variable	Distribution Type	Distribution Parameters
Failure time of DGs (h)	Exponential	$\lambda = 1.09 \times 10^{-3}$
Recovery time of DGs (h)	Weibull	$\alpha = 0.745$, $\beta = 6.14$
Battery life (h)	Triangular	(4, 5, 6)
SRV 1 fails open	Bernoulli	$p = 8.56 \times 10^{-4}$
Off-site AC power recovery (h)	Lognormal	$\mu = 0.793$, $\sigma = 1.982$
Clad fail temperature (F)	Triangular	(1800, 2200, 2600)
HPCI fails to run (h)	Exponential	$\lambda = 4.43 \times 10^{-3}$
RCIC fails to run (h)	Exponential	$\lambda = 4.43 \times 10^{-3}$
Battery failure time (h)	Exponential	$\lambda = 3.5 \times 10^{-6}$
Battery recovery time (min)[a]	Lognormal	$\mu = 45$, $\sigma = 15$
Firewater availability time (min)[a]	Lognormal	$\mu = 45$, $\sigma = 30$
Firewater flow rate (gal/min)	Uniform	(0, 200, 300)

[a]This parameter is related to human operations.

A summary of the distribution used is shown in Table II.

IV. SAFETY MARGIN ANALYSIS

This section shows some of the preliminary results regarding the effect of power uprates on the SBO accident scenario. A higher value of the thermal power generated in the core causes the following (see Fig. 8):

1. faster heating of the PSP and, thus, a reduction of the time interval between ADS activation time and loss of DG time, i.e., $T_{ADS} - T_{SBO}$
2. a faster core temperature increase rate after ADS activation; thus leading to less time available to the plant staff to align the FW.

In summary, we expect that a power uprate reduces the time available to the plant staff to recover AC power and the time available to the plant staff to align the FW. The scope of this section is to measure such reductions.

We performed an initial evaluation of the impact of power uprate by observing the PSP temperature increase rate as a function of the thermal power generated by the core (see Fig. 9a). In particular, we looked at the time to reach the PSP temperature limits for different values of core power (ranging from 100% to 120%). These results are shown in Fig. 9b. For this set of simulations, we fixed $T_{SBO} = 1$ h, and we, thus, measured $T_{ADS} - T_{SBO}$.

As expected, by increasing the core power, the time to reach the PSP heat capacity limits decreases. In Fig. 9a, the PSP temperature can be seen increasing in small steps as the SRVs open and close and remaining relatively flat for a longer period of time whenever HPCI/RCIC activates and it is unnecessary to open the SRVs for a longer period of time.

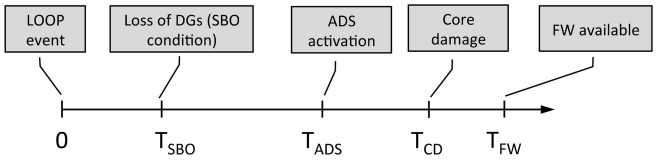

Fig. 8. Typical SBO sequence of events.

The sudden large increase in PSP temperature in each simulation is when the PSP heat capacity limit is reached and the ADS activates, dumping a huge amount of steam from the RPV into the PSP. Note that (Fig. 9b) if the reactor power is increased to 110% and 120%, the time to reach core HCTL limits decreases from 4.5 h (16 300 s) to 3.9 h (14 100 s) and 3.5 h (12 400 s), respectively.

Note that in this analysis we did not include an uncertainty study on some of the parameters characteristic of RELAP5-3D. Thus, the curve shown in Fig. 9b would not be shown as a single line, but it would be generated again through a stochastic sampling approach (described in Sec. II), and it would be shown as a "band" around the line shown in Fig. 9b. In this case, the margin (in terms of time to reach PSP HCTL) would no longer be deterministic but probabilistic and can be quantified though the methodology shown in Sec. II.

We then considered the impact of power uprate for the following cases:

1. time to activate ADS versus DG failure time (see Fig. 10a)
2. time to reach CD versus DG failure time (see Fig. 10b).

From Fig. 10 note the following:

1. We selected, for each power level (100%, 110%, and 120%), a set of values for T_{SBO}. We then ran a set of

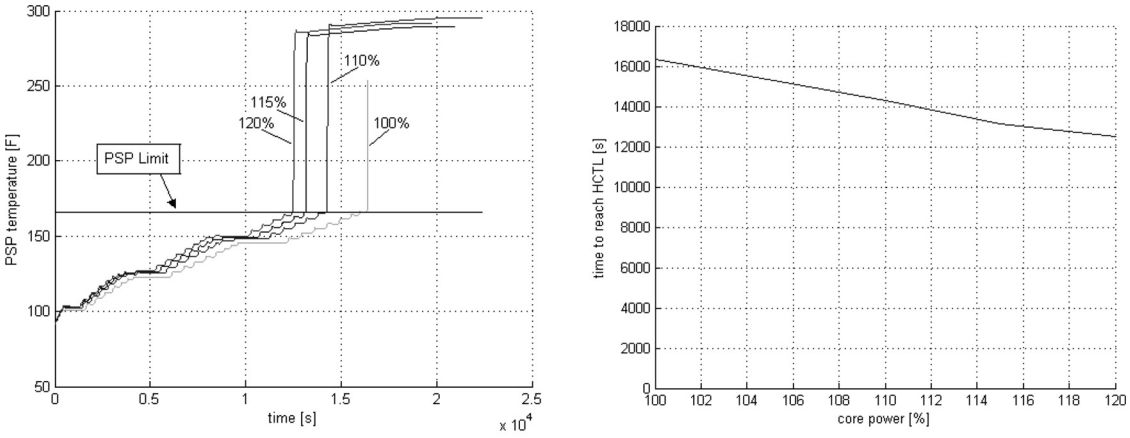

(a) (b)

Fig. 9. Impact of reactor power uprate on time to reach PSP heat capacity limits HCTL.

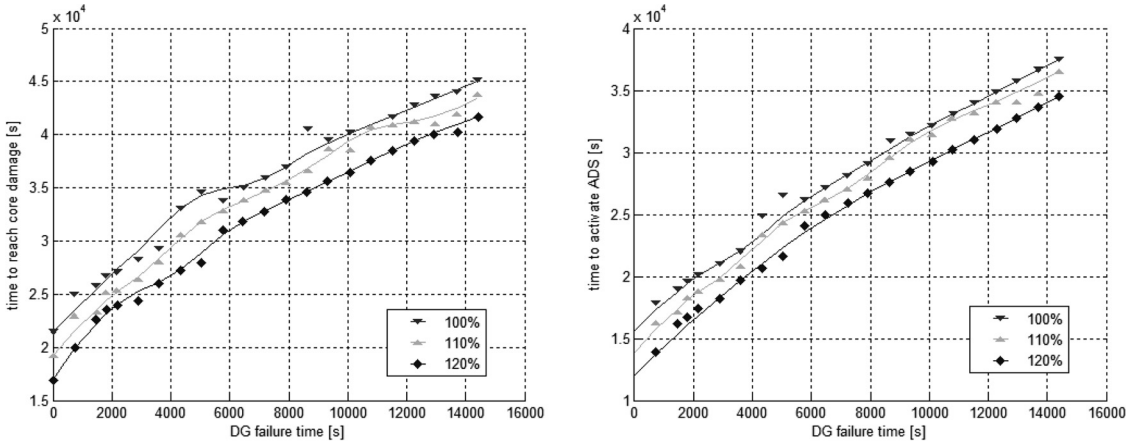

(a) (b)

Fig. 10. (a) Time to activate ADS versus DG failure time and (b) time to reach CD versus DG failure time curves, for 100% (top curves), 110% (middle curves), and 120% power (bottom curves).

simulation runs and identified that time at which the reactor operators needed to activate the ADS. Compared to what is presented in Fig. 9, this analysis considered not just PSP temperature as an indication to trigger ADS activation but all the curves shown in Fig. 4. In addition, AC power is not recovered, and FW is never available.

2. Figure 10a shows T_{SBO} (x-axis) versus $T_{ADS} - T_{SBO}$ (y-axis). By increasing T_{SBO}, we expect that the reactor operators are required to activate ADS much later. Again, a reactor power increase negatively affects ADS activation time.

3. Figure 10b shows T_{SBO} (x-axis) versus $T_{CD} - T_{SBO}$ (y-axis). If AC power is available for a long time, the PSP HCTL limits are reached further in time. This allows reaching CD much later.

V. STOCHASTIC ANALYSIS

We performed two series of Latin hypercube sampling analysis for the two levels of reactor power (100% and 120%) using 10 000 samples for each case. The scope of this analysis was to evaluate how CD probability changes when reactor power is increased from 100% to 120%. We also performed this analysis by identifying the importance of specific events by performing the following for each case:

1. building an ET-based logic structure that queries the following events: SRV status, DG, PG, and FW recovery (see Fig. 11)
2. associating each of the 10 000 simulations to a specific branch of the ET by querying the status of the SRV, PG, DG, and FW components in the simulation run

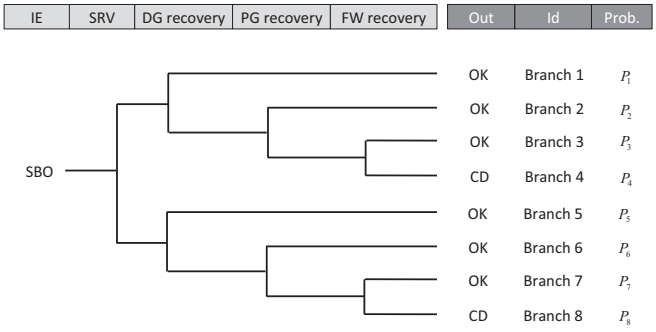

Fig. 11. Simplified ET logic structure for a BWR SBO.

TABLE III

Core Damage Probability for Two Different Power Levels (100% and 120%)

Outcome	100%	120%
OK	0.990	0.980
CD	9.82×10^{-3}	1.96×10^{-2}

3. evaluating the probability and the outcome associated with each branch.

A summary of the CD probability for the cases is shown in Table III: The probability value almost doubled for a 20% power increase. The summary of the branch probabilities represented in Fig. 11 is shown in Table IV. As expected, all branches that lead to CD have a probability increase while the ones leading to OK decrease. (Throughout, "OK" means "system success," i.e., no core damage.) Branch 4, which is the driving branch for the CD event, doubles its probability value.

As mentioned in Sec. IV, in this analysis we did not include an uncertainty study on some of the parameters characteristic of RELAP5-3D. However, since our analysis is stochastic and not deterministic, such uncertainty study would be represented as an additional dimension to be sampled in the RISMC approach.

Regarding the FW flow rate, we were able to determine that a minimum value of 50 gal/min is enough to assure an OK outcome if high-pressure injection is available, SRV stuck open failure does not occur, and DC batteries are always available. Note that branches 4 and 8 in Fig. 11 also include the simulations characterized by FW alignment before the CD condition is met but with the FW flow rate insufficient to keep the core cooled.

As second step in the analysis, we focused on the concept of limit surfaces[30]: the boundaries in the space of the sample parameters that separate failure from success. The advantage of limit surfaces is that they allow us to physically visualize how system performances are reduced due to, for example, a power uprate. By system performance, we mainly refer to both reduction in recovery timings (e.g., AC power recovery) and time reduction to perform steps in reactor operating procedures (e.g., time to reach HCTL).

For the scope of this paper, we focused on a safety-relevant case: DG failure time versus DG recovery time as shown in Fig. 12. These limit surfaces are obtained using support vector machine–based algorithms.[31] As expected, the failure region (light gray) expands when the reactor power is increased by 20%. This power increase on average reduces AC recovery time by ~1 h.

In addition to the analysis reported above, we evaluated the impact of auxiliary AC system generators as additional sources of AC power. The U.S. nuclear industry, as a measure after the Fukushima accident,[32] developed a FLEX system to counterattack the risks associated with external events (e.g., earthquakes or flooding). Such a system employs portable AC and DC emergency generators located not only within the plant perimeter but also at strategic locations within the U.S. borders in order to

TABLE IV

Branch Probabilities Associated with the ET Shown in Fig. 11 for Both Cases (100% and 120% Power)

Branch	Outcome	100%		120%		ΔP (%)
		Count	Probability	Count	Probability	
1	OK	3146	0.361	3238	0.353	−2.2
2	OK	4549	0.619	4440	0.617	−0.3
3	OK	847	0.00931	985	0.00926	−0.6
4	CD	557	0.00982	691	0.0196	+99
5	OK	333	7.32E-06	223	6.29E-06	−14
6	OK	254	1.53E-05	189	3.96E-06	−74
7	OK	251	5.92E-06	175	2.39E-06	−60
8	CD	63	2.12E-06	59	2.54E-06	+20

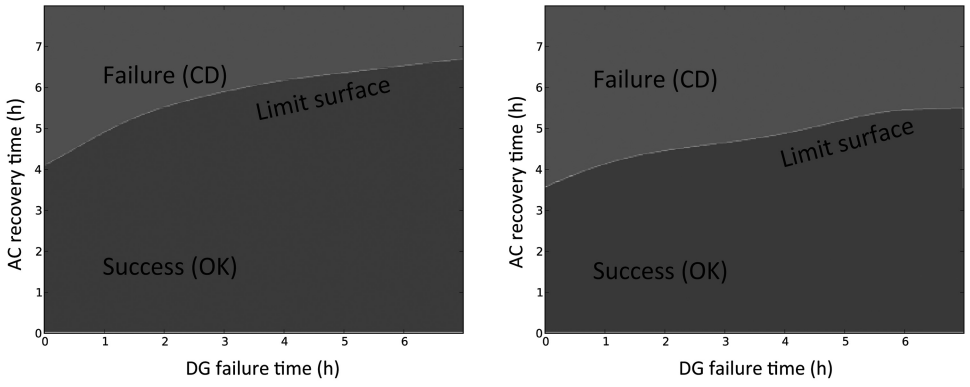

Fig. 12. Limit surface obtained in a two-dimensional space (DG failure time versus AC recovery time) for two different power levels: (a) 100% and (b) 120%.

TABLE V

Core Damage Probability for Two Different Test Cases (120% Without and With FLEX System)

Outcome	120% Without FLEX	120% With FLEX
OK	0.981	0.995
CD	1.96×10^{-2}	4.59×10^{-3}

quickly supply affected NPPs with both AC and DC power.

For our case, we assumed a new distribution associated with the AC recovery time within the plant instead of the DG recovery time distribution. Since FLEX operations can be considered as human-related events, we followed the same approach described in Sec. III.C for human-related events (see Table I). We assumed that the AC recovery can be considered to be of moderate complexity and high levels of stress/stressors. Note that this model may not be indicative of any actual NPP FLEX strategies—for an actual FLEX evaluation, plant-specific information would need to be considered. The new AC recovery distribution that replaces the DG recovery distribution is then a lognormal having mean and standard deviation values as follows:

1. mean = 15.0
2. standard deviation = 15.0.

We then performed a new Latin hypercube sampling analysis in order to estimate the new CD probability value and the branch probabilities associated with the ET structure shown in Fig. 11. Results are summarized in Tables V and VI. Note from Table V a decrease in CD probability because the new distribution has much lower mean value.

VI. CONCLUSIONS

In this paper we have shown the RISMC approach in order to evaluate the impact of power uprate on a BWR SBO accident scenario. We have employed RELAP5-3D

TABLE VI

Branch Probabilities for Two Different Test Cases (120% Without and With FLEX System)

Branch	Outcome	Probability (120%)		ΔP (%)
		Without FLEX	With FLEX	
1	OK	0.353	0.505	43
2	OK	0.618	0.490	−21
3	OK	0.009258	3.49E-05	−100
4	CD	0.0196	0.00459	−77
5	OK	6.29E-06	2.87E-06	−54
6	OK	3.96E-06	1.79E-09	−100
7	OK	2.39E-06	6.77E-10	−100
8	CD	2.54E-06	1.09E-09	−100

as the system simulator code and the RAVEN code to perform the accident sequence generation and statistical analysis. The BWR system, the system control logic, and the accident scenario have been directly implemented in the RELAP5-3D input file. We evaluated the increase of CD probability of such power uprate and its decrease due to the implementation of the FLEX system to provide emergency power to the plant. In particular, we have shown how the RISMC approach to perform PRA analyses can provide the user a much larger amount of information such as time reduction for plant recovery strategies.

This paper also aims to answer the question: Are the efforts (from a modeling and computational point of view) required by the RISMC approach worth the results that can be obtained using state-of-practice methodologies? We believe that simulation-based methods are the natural extension of traditional methods. This extension aims to overcome the natural limitations of the latter ones such as user-defined accident progression and the lack of system dynamic feedback into the timing/sequencing of events. Phenomena such as power uprate could only be considered in the actual approximated computation of the ET branches or FT basic event probabilities without modeling their actual feedback on timing/sequencing of events.

Acknowledgment

This work was accomplished through the RISMC pathway as part of the U.S. Department of Energy LWRS program.

References

1. C. SMITH, C. RABITI, and R. MARTINEAU, "Risk Informed Safety Margins Characterization (RISMC) Pathway Technical Program Plan," INL/EXT-11-22977, Idaho National Laboratory (2011).
2. "Light Water Reactor Sustainability Program and EPRI Long-Term Operations Program—Joint Research and Development Plan," INL-EXT-12-24562, Rev. 3, Idaho National Laboratory (2014).
3. "Severe Accident Risks: An Assessment for Five U.S. Nuclear Power Plants," NUREG 1150, U.S. Nuclear Regulatory Commission (1990).
4. "Reactor Safety Study—An Assessment of Accident Risks in U.S. Commercial Nuclear Power Plants," WASH 1400, U.S. Nuclear Regulatory Commission (1975).
5. "Safety Margin Evaluation—SMAP Framework Assessment and Application," NEA/CSNI/R(2011)3, Organisation for Economic Co-operation and Development/Nuclear Energy Agency, Committee on the Safety of Nuclear Installations (2011).
6. V. N. DANG and D. R. KARANKI, "Modeling Operator Actions in Integrated Deterministic-Probabilistic Safety Assessment," *Proc. Probability Safety Assessment and Management Conf.* (*PSAM 12)*, Honolulu, Hawaii, June 22–27, 2014.
7. V. RYCHKOV and M. SALMAOUI, "Risk Informed Safety Margins Characterization via Failure Domain Quantification. Loss of Main Feed Water Example," *Proc. Int. Topl. Mtg. Probabilistic Safety Assessment and Analysis (PSA 2013)*, Columbia, South Carolina, September 22–27, 2013, American Nuclear Society (2013).
8. K. METZROTH and T. ALDEMIR, "The ADAPT Framework for Dynamic Probabilistic Safety Assessment," *Proc. Integrated Deterministic-Probabilistic Safety Analysis Workshop (IDPSA-2012),* Stockholm, Sweden, November 19–21, 2012, KTH (2012).
9. E. ZIO, "Integrated Deterministic and Probabilistic Safety Analysis: Concepts, Challenges, Research Directions," *Nucl. Eng. Des.*, **280**, 413 (2014); http://dx.doi.org/10.1016/j.nucengdes.2014.09.004.
10. RELAP5 CODE DEVELOPMENT TEAM, "RELAP5-3D Code Manual," INEEL-EXT-98-00834, Idaho National Laboratory (2012).
11. A. DAVID et al., "RELAP-7 Level 2 Milestone Report: Demonstration of a Steady State Single Phase PWR Simulation with RELAP-7," INL/EXT-12-25924, Idaho National Laboratory (2012).
12. B. SPENCER et al., "Grizzly Year-End Progress Report," INL/EXT-13-30316, Idaho National Laboratory (2013).
13. C. RABITI et al., "Deployment and Overview of RAVEN Capabilities for a Probabilistic Risk Assessment Demo for a PWR Station Blackout," INL/EXT-13-29510, Idaho National Laboratory (2013).
14. C. RABITI et al., "Mathematical Framework for the Analysis of Dynamic Stochastic Systems with the RAVEN Code," *Proc. Conf. Mathematics and Computational Methods Applied to Nuclear Science and Engineering (M&C 2013)*, Sun Valley, Idaho, May 5–9, 2013, American Nuclear Society (2013).
15. E. ZIO et al., "A Concept Paper on Dynamic Reliability via Monte Carlo Simulation," *Math. Comput. Simul.*, **47**, 371 (1998); http://dx.doi.org/10.1016/S0378-4754(98)00112-8.
16. J. C. HELTON and F. J. DAVIS, "Latin Hypercube Sampling and the Propagation of Uncertainty in Analyses of Complex Systems," *Reliab. Eng. Syst. Saf.*, **81**, *1*, 23 (2003); http://dx.doi.org/10.1016/S0951-8320(03)00058-9.
17. A. AMENDOLA and G. REINA, "Dylam-1, A Software Package for Event Sequence and Consequence Spectrum Methodology," EUR-924, CEC-JRC, ISPRA: Commission of the European Communities (1984).
18. N. V. QUEIPO et al., "Surrogate-Based Analysis and Optimization," *Prog. Aerospace Sci.*, **41**, 1 (2005), http://dx.doi.org/10.1016/j.paerosci.2005.02.001.

19. A. ALFONSI et al., "RAVEN as a Tool for Dynamic Probabilistic Risk Assessment: Software Overview," *Proc. Conf. Mathematics and Computational Methods Applied to Nuclear Science and Engineering (M&C 2013)*, Sun Valley, Idaho, May 5–9, 2013, American Nuclear Society (2013).
20. C. RABITI et al., "Advanced Probabilistic Risk Analysis Using RAVEN and RELAP-7," INL/EXT-14-32491, Idaho National Laboratory (2014).
21. A. ALFONSI et al., "RAVEN: Dynamic Event Tree Approach," INL/EXT-13-30332, Idaho National Laboratory (2013).
22. D. MANDELLI et al., "Support and Modeling for the Boiling Water Reactor Station Black Out Case Study Using RELAP and RAVEN," INL/EXT-13-30203, Idaho National Laboratory (2013).
23. D. H. COOK et al., "Station Blackout at Browns Ferry Unit One—Accident Sequence Analysis," NUREG/CR-2182, Vol. 1, U.S. Nuclear Regulatory Commission, Office of Nuclear Regulatory Research (1981).
24. S. EIDE et al., "Reevaluation of Station Blackout Risk at Nuclear Power Plants," NUREG/CR-6890, Vol. 1, "Analysis of Loss of Offsite Power Events: 1986–2004," U.S. Nuclear Regulatory Commission (2005).
25. S. EIDE et al., "Reevaluation of Station Blackout Risk at Nuclear Power Plants," NUREG/CR-6890, Vol. 2, "Analysis of Station Blackout Risk," U.S. Nuclear Regulatory Commission (2005).
26. R. R. SHERRY, J. R. GABOR, and S. M. HESS, "Pilot Application of Risk Informed Safety Margin Characterization to a Total Loss of Feedwater Event," *Reliab. Eng. Syst. Saf.*, **117**, 65 (2013); http://dx.doi.org/10.1016/j.ress.2013.03.018.
27. "State-of-the-Art Reactor Consequence Analysis (SOARCA) Project Surry Integrate Analyses Report," NUREG/CR-7110, Vol. IV, U.S. Nuclear Regulatory Commission.
28. D. GERTMAN et al., "NUREG/CR-6883: The SPAR-H Human Reliability Analysis Method," U.S. Nuclear Regulatory Commission (2005).
29. D. MANDELLI et al., "Risk-Informed Safety Margin Characterization Methods: Development Work," INL/EXT-14-33191, Idaho National Laboratory (2014).
30. D. MANDELLI and C. SMITH, "Adaptive Sampling Using Support Vector Machines," *Trans. Am. Nucl. Soc.*, **107**, 736 (2012).
31. C. J. C. BURGES, "A Tutorial on Support Vector Machines for Pattern Recognition," *Data Min. Knowl. Discov.*, **2**, 121 (1998); http://dx.doi.org/10.1023/A:1009715923555.
32. "Special Report on the Nuclear Accident at the Fukushima Daiichi Nuclear Power Station," INPO Report 11-005, Institute of Nuclear Power Operations (2011).